

## VISCOUS LIQUID AIR-MIXING: INFLUENCE OF LIQUID DENSITY RATIO

**Mahesh PRAKASH<sup>1</sup>, Ben KORMAN<sup>2</sup> and Paul W. CLEARY<sup>1</sup>**

<sup>1</sup>CSIRO Mathematics, Informatics and Statistics, Private Bag, Clayton South, Victoria 3169, AUSTRALIA

<sup>2</sup>Department of Mechanical Engineering, Monash University, Victoria 3800, AUSTRALIA

### ABSTRACT

The mixing of multiple viscous liquids with different densities (e.g. paints) in the presence of an air gap, by means of a rotating shaker is explored numerically using the mesh-free Smoothed Particle Hydrodynamics (SPH) method. SPH is used to predict the effect on mixing performance of varying the density ratio between the liquids. To facilitate mixing, the shaker contains an air gap which provides headspace in which blending occurs. The liquids occupy 50% of the volume of the shaker. Mixing between the two liquids occurs due to interface stretching and folding caused by their periodic rise and fall, forming plume like protrusions at the free surface. The efficiency of the mixing process is governed by the rate at which the unmixed liquids are transported as thin jets along the side walls of the shaker. It was observed that the greater the difference in density between the two liquids, the less efficient their transportation to the mixing zone becomes, thereby reducing the rate of mixing. Below a density ratio of 0.7, mixing is practically non-existent. Above this value the rate of mixing follows a quadratic trend.

### INTRODUCTION

Liquid mixing and blending is of great importance to many different industries including pharmaceuticals, petrochemicals, bioengineering, paints, cosmetics and the food industry. These applications require highly viscous or non-Newtonian liquids to be mixed. This is achieved through specialised mixing or blending equipment. A commonly used machine for applications such as paint mixing is a shaker, due to its relative cost effectiveness (See Figure 1). A shaker is a container commonly attached to either one or two moving brackets. This container is then agitated by following either a simple two dimensional or more complex three dimensional path.

When two liquids are mixed, the time taken for them to blend (Boumans et al., 1990) and the extent to which they blend (Boumans et al., 1997) is largely governed by their viscosity and density differences. When mixing two liquids of different densities, the variation in densities in combination with inadequate motion of the container can result in excessively long mixing times. This is highly undesirable both economically and logistically with an estimated cost to industry due to a lack of knowledge in this area of about USD10 billion per year in the USA alone (Smith, J.M., 1990).

To facilitate mixing, the shaker must also contain an air gap which provides space for blending to occur. A numerical analysis of such mixing and blending must be modelled using a multi-phase flow method that can simulate large density differences.

Until recently, the SPH method has only been used for solving multi-fluid flows when the ratio of fluid densities

is relatively low. Monaghan and Kocharyan (1995) modelled a dusty gas flow and Monaghan et al. (1999) simulated gravity currents using density ratios of less than 20:1. Larger density differences were reported to lead to instabilities across the fluid interfaces for these systems. This meant that a system containing air (with a density of  $1 \text{ kg/m}^3$ ) and liquid (typically with a density of  $1000 \text{ kg/m}^3$ ) could not be solved by SPH with sufficient accuracy. Colagrossi and Landrini (2003) modified the standard SPH method to resolve this problem and successfully applied it to a 2D dam break and a 2D air bubble rising in a box containing a liquid. In both these instances the geometry was simple and stationary. Their modifications to the standard SPH formulation included a new form of the particle evolution equation derived following Bonet and Lok (1999), periodic re-initialization of the density field based on a moving least squares interpolation and a correction to the artificial viscosity term as presented in Benz (1990). Prakash and Cleary (2009) recently modified the SPH method to simulate multi-fluid flows with large density differences where there is significant free surface deformation as well as moving geometry.

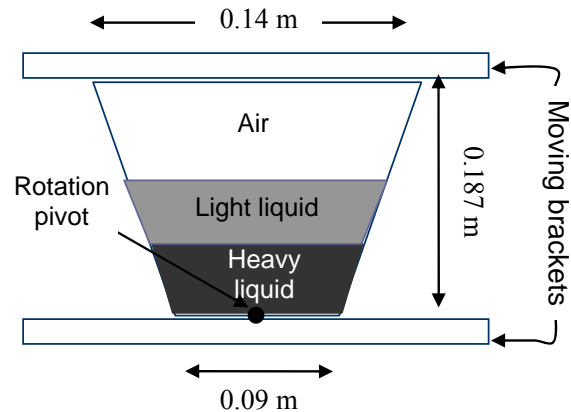


**Figure 1:** Schematic of the shaker used for viscous liquid mixing.

### MODEL DESCRIPTION

The SPH methodology used here is a modified form of the standard weakly compressible formulation presented in Monaghan (1992). The modifications are necessary for multi-phase fluid flows with large density differences. A detailed description of the modified method is presented in Prakash and Cleary (2009). Here we present a summary of the methodology and the key modifications.

In SPH the interpolated value of a function  $A$  at any position  $\mathbf{r}$  can be expressed using SPH smoothing as (Monaghan, 1992):

$$A(\mathbf{r}) = \sum_b m_b \frac{A_b}{\rho_b} W(\mathbf{r} - \mathbf{r}_b, h) \quad (1)$$

where  $m_b$  and  $\mathbf{r}_b$  are the mass and density of particle  $b$  and the sum is over all nodes within a radius  $2h$  of  $\mathbf{r}$ . Here  $W(\mathbf{r}, h)$  is a  $C^2$  spline based interpolation or smoothing kernel with radius  $2h$  that approximates the shape of a Gaussian function. The gradient of the function  $A$  is given by differentiating the interpolation equation (1) to give:

$$\nabla A(\mathbf{r}) = \sum_b m_b \frac{A_b}{\rho_b} \nabla W(\mathbf{r} - \mathbf{r}_b, h) \quad (2)$$

Using these interpolation formulae and suitable finite difference approximations for second order derivatives, one is able to convert parabolic partial differential equations into ordinary differential equations for the motion of the nodes and the rates of change of their properties.

### Momentum and Continuity Equations

Based on the above interpolation formulae, the modified SPH momentum equation for dealing with density discontinuities can be written as:

$$\frac{d\mathbf{v}_a}{dt} = \mathbf{g} - \sum_b \frac{m_b}{\rho_a \rho_b} \left[ \left( \frac{P_b}{\rho_b^2} + \frac{P_a}{\rho_a^2} \right) \frac{A_b \mu_a \mu_b}{(\mu_a + \mu_b)} \frac{\mathbf{v}_a \mathbf{r}_{ab}}{r_{ab}^2 + r^2} \right] \nabla_a W_{ab} \quad (3)$$

where  $\bar{\rho} = \rho / \rho^o$  is the ratio of the reference density (the actual fluid density) and the density calculated from the weakly compressible formulation.

In a similar manner to the momentum equation, the modified continuity equation can be written as:

$$\frac{d\rho_a}{dt} = \sum_b \frac{\rho_a^o}{\rho_b^o} m_b (\mathbf{v}_a - \mathbf{v}_b) \nabla W_{ab} \quad (4)$$

The above form correctly enforces continuity across interfaces between fluids with substantially different densities.

### Equation of State

Since SPH is weakly compressible, an equation of state is needed to relate the pressure to the density fluctuations. Two slightly different formulations are used here for the equation of state in the viscous liquids and air. This allows the SPH speed of sound to be the same in both air and liquids. In order to stabilise their solution Colagrossi and Landrini (2003) used approximately 10 times the speed of sound in air compared to the speed of sound in the liquid. Here, by using both the smaller sound speed and the same value for both fluids, a 10 fold increase in time-step is achieved. Additionally, the current formulation does not use any density re-initialisation as needed for the model presented by Colagrossi and Landrini (2003).

The incompressibility in the liquid is achieved by setting the speed of sound in such a way that the maximum flow velocity in the liquid is less than 10% of the SPH sound speed. This results in the liquid being less than 1% compressible. In our computations the liquid compressibility was typically less than 0.6% whereas the air was found to be around 2% compressible. Details of the equations of state used can be found in Prakash and Cleary (2009).

## GEOMETRY, MODEL SETUP AND MIXING MEASURES

The geometry of the setup used for performing mixing and blending simulations is presented in Figure 1. The height of the container is 0.187 m, its width is 0.09 m at the bottom and 0.14 m at the top. It has an air gap above the liquid whose fill level is 50%. The liquid initially at the bottom has viscosity  $\mu = 2.0$  Pa and density  $\rho_H = 1000$  kg/m<sup>3</sup> and the liquid initially at the top has viscosity  $\mu = 2.0$  Pa and a density which is varied from  $\rho_L = 1000$  kg/m<sup>3</sup> to 100 kg/m<sup>3</sup>. 9000 SPH particles with a size of 1.5 mm are used to represent the fluid (air and liquids) in this two dimensional system. The brackets housing the container have a rotational path described by:

$$f(t) = -0.5 A_h \omega^2 \sin(\omega t) \mathbf{e}_x + 0.5 A_v \omega^2 \cos(\omega t) \mathbf{e}_y \quad (5)$$

where  $A_h = A_v =$  amplitudes in the horizontal and vertical direction in m.  $\omega = 20\pi$  s<sup>-1</sup> (equivalent to 10 RPS) and  $\mathbf{e}_x$  and  $\mathbf{e}_y$  are unit vectors in the horizontal and vertical direction. The centre of rotation is located at the bottom of the container as shown in Figure 1.

There are a range of methods for characterising liquid mixing in such systems. These vary from tracking the centroid of different parts of the liquid with time as presented in Cleary et al. (2002), through to the finite time Lyapunov exponent measure of mixing as applied to the twin-cam mixer by Robinson et al. (2008). In many mixing applications the degree of homogenisation of a particular inert species (such as a tracer dye) or non-inert species (such as a reactant) is employed to quantify the mixing process (Yeoh et al., 2005 and Zhang et al., 2009). For the present analysis, the liquid domain is divided into two equal volume horizontal strata. The  $y$  co-ordinate location of the centroid of the two liquids is calculated with time. A fully mixed liquid will have both centroids coincident with the overall centre of mass of the liquid. The percentage of mixing at any time is calculated with the following equation:

$$\text{Mix}(\%) = \frac{X_{start} - x_{present}}{X_{start} - X_{overall}} \times 100 \quad (6)$$

where  $X_{start}$  = monitored co-ordinate of centroid location of each liquid strata at  $t = 0$ .

- $X_{overall}$  = monitored co-ordinate of centroid location of overall liquid centre of mass and
- $x_{present}$  = monitored co-ordinate of current centroid location of each liquid strata.

Each simulation is run until the level of mixing measure has stabilised to a steady value meaning that further mixing has ceased.

## RESULTS

### Flow and velocity pattern in shaker

The development of the flow pattern in the shaker is shown in Figure 2 with both liquids of the same density. At each time there is a pair of pictures with the fluids coloured by velocity on the left and by their material colour on the right. For the fluids coloured by speed, blue represents 0.0 m/s and red represents 1.5 m/s. Velocity vectors are plotted for every 8<sup>th</sup> fluid particle to show the direction of motion of the fluid. The length of the arrow depends on the magnitude of velocity. For pictures coloured by material type, grey indicates the viscous liquids whereas white indicates the air layer on top.

In the first cycle (between 0.0 and 0.1 s) the fluid has just started responding to the shaker motion as seen from the mild deformation in the free surface shape. At 0.01 s the shaker has just started moving around its pivot. At 0.04 s the liquid is moving to the left in the same direction as the shaker. A low velocity re-circulation cell is created close to the interface between the air and liquid. The liquid free surface deforms and rises up near the right wall of the shaker.

At 0.08 s the fluid is moving to the right with the shaker. The slow moving re-circulation cell at the interface between the liquid and the air persists but has moved to the left. The liquid interface is starting to deform about the re-circulation cell at this time. The presence of the re-circulation zone helps to promote interface stretching and folding. At 0.10 s the shaker is back to its original position. The bulk of the fluid is now moving up with the shaker at a velocity of around 1.0 m/s. The interface distortion is relatively weak at this stage due to the absence of a clearly established re-circulation zone.

After around 20 rotations the fluid flow pattern in the shaker becomes periodic. This is established from the periodicity seen in the velocity and flow patterns. At 2.0 s, fluid in the shaker is moving upward. The air close to the centre of the shaker moves upwards with a high velocity of around 1.5 m/s. The liquids, being much denser, push the air around. The liquid interface deforms around the low velocity re-circulation cell on the right due to the change in the direction of fluid motion in this region. The small region of low velocity close to the left wall has only a minor effect in deforming the liquid interface in this section.

At 2.04 s the shaker is moving on a downwards trajectory. The air closer to the left wall of the shaker almost immediately moves down with the shaker at high velocity as shown by the red colour of the fluid in the top left corner. The lower half of the liquid still moves with the shaker and has a velocity of less than 1.0 m/s. A central re-circulation region can be seen. The liquid interface on the right is deformed around this structure. At 2.08 s, the shaker is moving from left to right. The air in the top half moves with the shaker at a high velocity of around 1.5 m/s. The low velocity re-circulation cell on the left has the effect of deforming the liquid interface adjacent to it creating a liquid plume.

At 2.10 s, the shaker has once again moved back to its original position with an upward trajectory. The air on the left moves up at a high velocity with the shaker. The low velocity re-circulation cell is once again visible near the centre of the shaker, driving further deformation of the liquid interface.

In summary, once the flow establishes itself with a periodic pattern, the flow field develops re-circulation cells that change in number and position with time. These cells have the effect of deforming the liquid interface. The size of these cells determines the degree to which they can distort the liquid interface, which in turn controls the stretching and folding of the liquids leading to mixing. The mobility of these cells over the shaker cycle seems to influence the degree of mixing.

#### Variation in flow and mixing pattern with density

The variation in flow and mixing behaviour with changes in the density ratio is shown in Figure 3. The columns

represent density ratios 1.0, 0.9, 0.8, 0.7 and 0.1 from left to right. The rows represent duration of mixing non-dimensionalised by the shaker rotation cycle time. The mixing pattern is compared here at 50, 100, 200, 400 and 600 cycles. From the start of the shaker motion the liquid gradually gains momentum. In Figure 3(a) for  $\rho_L/\rho_H = 1.0$ , the liquid free surface begins to deform appreciably after 50 cycles creating a wave pattern. The peaks of these waves rise and fall back into the liquid. This process results in rapid mixing in the surface region. After 50 shaker cycles for  $\rho_L/\rho_H = 1.0$ , a clear jet of liquid is transported along the left wall from the unmixed lower half into the folding and stretching flow at the air-liquid interface. The rate at which this transfer occurs limits the rate of mixing since the liquids are rapidly mixed once they enter the surface mixing region. After 200 shaker cycles, as a result of this transportation and mixing, around a quarter of the blue layer has mixed with the top red liquid. Liquid droplets thrown into the air layer, further enhances mixing.

At 400 and 600 shaker cycles, a second downward directed jet along the right wall can be seen which draws air from the head space and transports it into the surface mixing region. The jet of liquid from the lower unmixed region and the air jet together create a clockwise re-circulation of the liquid in the top half. The rate of mixing is therefore controlled by the strength of the jets which transport gas from above and liquid from below making them available for mixing in the top liquid layer.

At lower density ratios the mechanism of mixing can be seen to be similar to that just described for equal densities. However the size of the mixing zone, the rate of mixing and the rate of transportation of liquid into the surface mixing region decreases progressively with a reduction in the density ratio.

In Figure 3(b) for  $\rho_L/\rho_H = 0.9$  the liquid free surface is deformed to a lesser degree than  $\rho_L/\rho_H = 1.0$  due to the lighter liquid at the top having a lower momentum and thereby reduced inertia. The pressure (exerted by the lighter liquid on the heavy liquid) reduces leading to reduced interface deformation. This in turn decreases the size of the waves at the air-liquid interface. From Figure 3(b) to (e) the size of these waves at the liquid free surface diminish progressively. The strength of the peaks of waves rising and falling back into the liquid consequently reduces thereby diminishing the size of the surface mixing layer.

The reduced inertia of the lighter liquid also results in longer times required for the liquid free surface to respond to the shaker motion. For example, significant liquid deformation occurs as early as 50 cycles for  $\rho_L/\rho_H = 1.0$  and 0.9 in comparison to the 200 cycles required for  $\rho_L/\rho_H = 0.8$  and 0.7. The deformation is very weak for  $\rho_L/\rho_H = 0.1$  even after 600 cycles. The slower rate of interface deformation results in reduced mixing rates at low density ratios.

A secondary effect of the reduction in the liquid interface deformation is the reduced ability of gas from the headspace to entrain into the liquid along the right wall as thin jets. In fact the gas entrainment becomes insignificant at  $\rho_L/\rho_H = 0.9$  as seen from Figure 3(b) and is non-existent for  $\rho_L/\rho_H = 0.8$  and onwards.

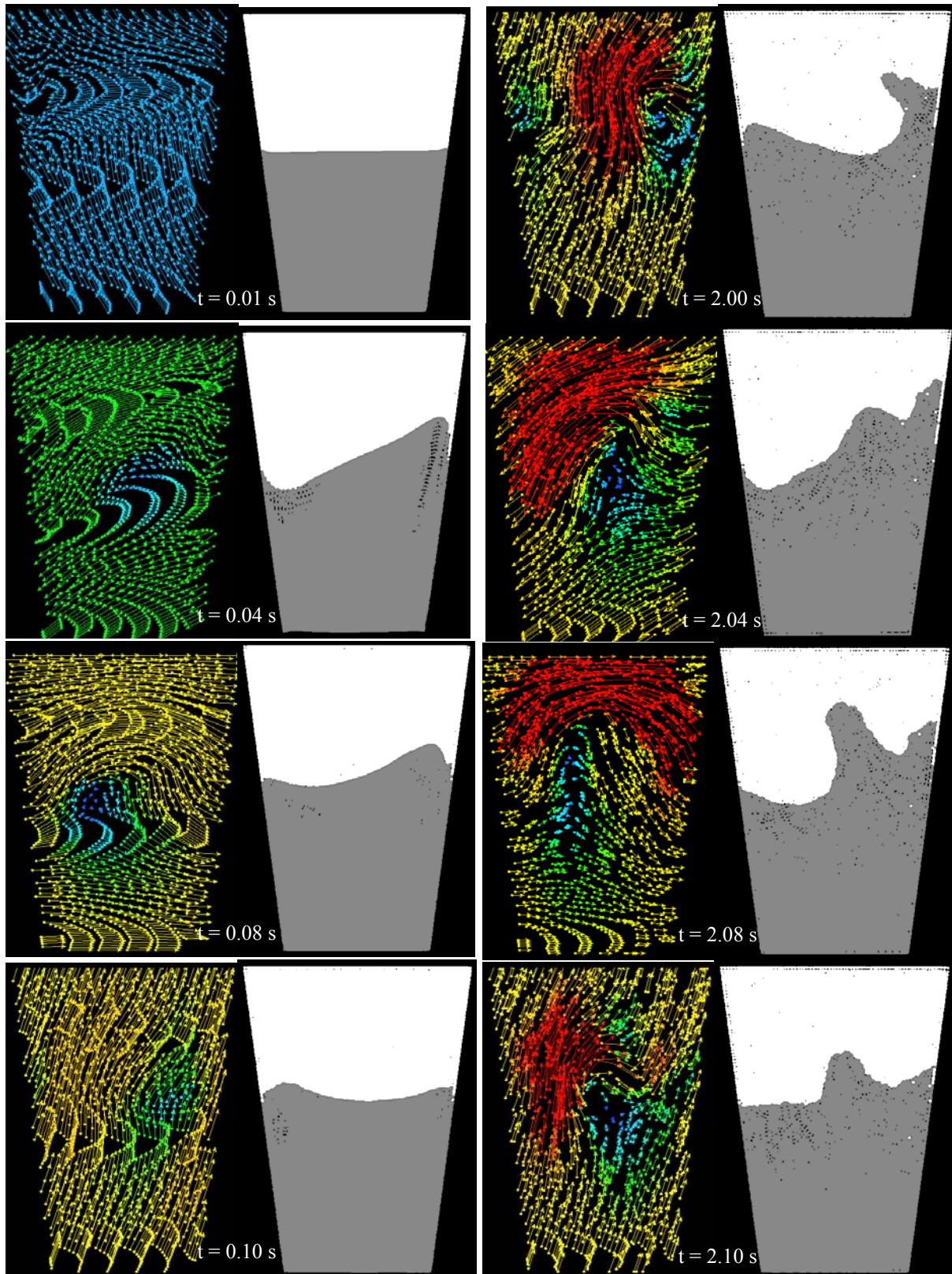


**Figure 2:** Flow and mixing pattern in the shaker for a 50% viscous liquid fill level and  $\rho_l/\rho_H = 1.0$ . At each time there is a pair of pictures with the fluid coloured by velocity on the left and by its material type on the right. For velocity colouring, blue indicates 0.0 m/s and red indicates 1.5 m/s. The white fluid is air whereas the grey coloured fluid is the viscous liquid. It takes 0.1 s for one shaker cycle. A periodic flow pattern develops after 2.0 s.

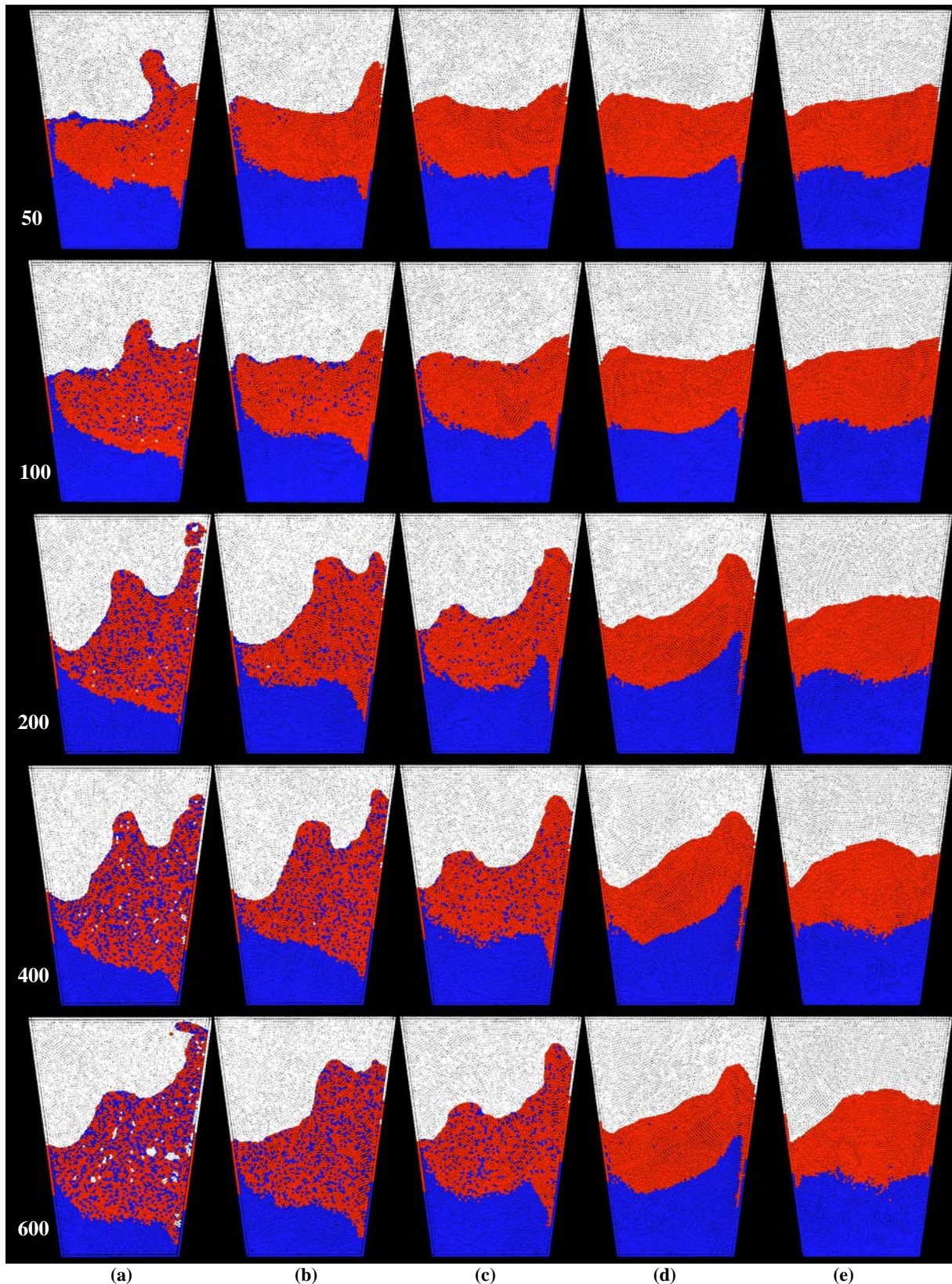


**Figure 3:** Mixing between two liquids, with density ratio  $\rho_L/\rho_H =$  (a) 1.0 (b) 0.9 (c) 0.8 (d) 0.7 and (e) 0.1. The heavier liquid ( $\rho_H$ ) is coloured blue and the lighter liquid ( $\rho_L$ ) is coloured red. The air pocket at the top is coloured white. The rows represent duration of mixing non-dimensionalised by the shaker rotation cycle time. The mixing pattern is compared at 50, 100, 200, 400 and 600 cycles.

Comparing Figures 3(a) and (b) at 50 cycles shows that the size of the jet of heavy liquid close to the left wall of the shaker is significantly less for  $\rho_L/\rho_H = 0.9$  when compared to a density ratio of 1.0. This decreases further for  $\rho_L/\rho_H = 0.8$  and is non-existent for  $\rho_L/\rho_H = 0.7$  and 0.1. The buoyant light liquid acts to restrict the transport of heavier liquid into the surface mixing zone. Mixing in these systems requires both stretching and folding of the liquid free surface resulting in the creation of an active surface mixing zone and a well established transportation mechanism capable of injecting unmixed liquid into the mixing zone.

For the cases reported here the impedance due to buoyancy almost completely cuts off the transportation of the heavy liquid at  $\rho_L/\rho_H = 0.7$ . As shown in Figure 3(d) there is very little transportation of blue liquid into the surface mixing zone even after 600 shaker cycles and therefore, practically no mixing occurs between the two liquids.

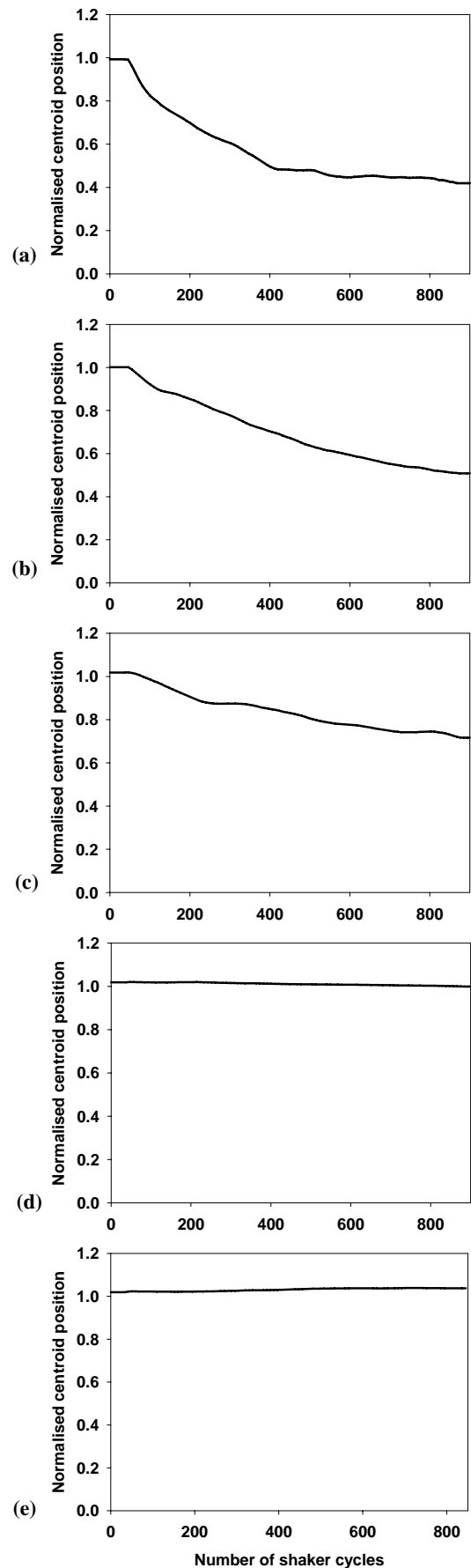
#### Degree of mixing

Figure 4 shows the change in the normalised centroid position of the two liquids for different density ratios. For  $\rho_L/\rho_H = 1.0$  in 40 shaker rotation cycles there is minimal change in the degree of mixing. There is a significant increase in the rate of mixing between 40 and 400 shaker cycles when the centroid moves from 1.0 to 0.48. This rapid mixing stage can be attributed to the transportation of liquid jets to the top mixing layer and air entrainment into the mixing zone which further enhances mixing. Between 400 and 550 cycles the degree of mixing between the liquids slows down. The mixing then continues gradually with the centroid dropping from 0.48 to 0.40 between cycles 550 to 900. By 900 cycles the two liquids are essentially mixed to their maximum extent for this density ratio.

For  $\rho_L/\rho_H = 0.9$ , there is minimal mixing over the first 35 cycles, after which mixing begins and continues until around 800 shaker cycles. The mixing follows a logarithmic trend, initially fast, but decaying rapidly at around 700 shaker cycles. After 800 cycles, the centroid is at 0.48 and there is practically no further mixing.

For  $\rho_L/\rho_H = 0.8$ , no mixing is evident until 40 shaker cycles. The mixing rate then follows an almost linear trend until around 230 shaker cycles, at which point the centroid has fallen to 0.85. Between 230 and 380 cycles the mixing rate is very slow. The two liquids continue to mix with a reduced linear rate between 380 and 630 cycles. The centroid is at 0.76 after 630 cycles when the rate is further reduced with very gradual mixing between the two liquids. The centroid is at 0.70 at 900 cycles for this case.

For density ratios below 0.8, there is a severe deterioration in the rate of mixing between the two liquids. This can be seen from the centroid measure for  $\rho_L/\rho_H = 0.7$  in Figure 4(d) where there is no change in the centroid position even after 900 shaker rotation cycles. This trend continues for lower density ratios. The lowest density ratio examined in this study,  $\rho_L/\rho_H = 0.1$  in Figure 4(e), shows a similar mixing profile.



**Figure 4:** Change in centroid position with shaker rotation cycle for  $\rho_H/\rho_L =$  (a) 1.0 (b) 0.9 (c) 0.8 (d) 0.7 and (e) 0.1.

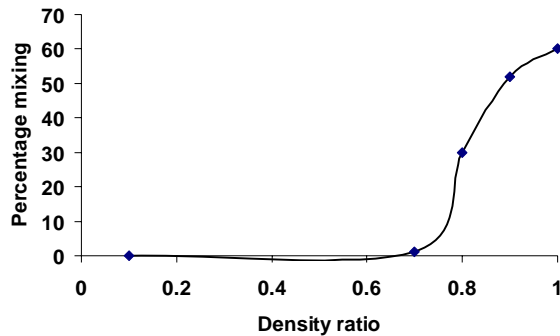


**Figure 5:** Change in percentage mixing with density ratio between the lighter and heavier liquid after the mixing has reached its asymptotic limit.

From the analysis of surface mixing and transportation it is clear that in going from a density ratio of 0.8 to 0.7 there is no significant change in the degree of stretching and folding of the liquid free surface. However the change in buoyancy of the lighter liquid becomes sufficient to prevent any transportation of the heavy liquid into the surface mixing zone. This reduces the mixing rate significantly and prevents any mixing between the two liquids.

A plot of the density ratio between the two liquids and the percentage mixing is shown in Figure 5. There is no mixing between the two liquids for density ratios 0.7 or less. Above this value the degree of mixing follows a quadratic trend with the density ratio:

$$Mix_{deg} = -5.2 \left( \frac{\rho_L}{\rho_H} \right)^2 + 1.08 \left( \frac{\rho_L}{\rho_H} \right) - 5.04 \quad (7)$$

## CONCLUSIONS

The SPH method is applied to analyse the effect of density ratio on mixing between two viscous liquids. Three zones are clearly seen in the shaker during the mixing:

- An upper re-circulating mixing zone close to the interface between the liquid and the gas where the stretching and folding of the liquid interface causes rapid mixing.
- Thin jets of liquid from the lower unmixed region and gas from the air space flow along the side walls of the shaker and into the mixing zone. The rate of transportation of material from these jets into the mixing region determines the rate of mixing.
- A lower unmixed liquid region which acts as a reservoir of liquid from where it is transported as thin jets to the upper mixing zone.

With a reduction in the density ratio the lighter liquid shows decreased momentum and inertia. This results in less stretching and folding of the liquid free surface thereby leading to a drop in the size of the surface mixing layer. The reduced inertia also results in increased times required for the liquid free surface to respond to the shaker motion thereby reducing the mixing rates.

At lower density ratios the upper light liquid becomes more buoyant thereby greatly impeding the transportation of the heavy liquid into the mixing layer. Below a density ratio of 0.7 the impedance due to buoyancy almost completely cuts off the transportation of the heavy liquid into the mixing zone. Above this value the mixing follows a quadratic trend.

## REFERENCES

- BENZ, W., (1990). Smooth particle hydrodynamics: a review. in: *J.R. Buchler (Ed.), The Numerical Modelling of Nonlinear Stellar Pulsation*, Kluwer Academic Publishers, Dordrecht, 269–288.
- BONET, J. and LOK, T. S. L., (1999). Variational and momentum preservation aspects of SPH formulations. *Comput. Methods Appl. Mech. Eng.*, 180, 97–115.
- BOUWMANS, I., BAKKER, A. and VAN DEN AKKER, H. E. A. (1997). Blending liquids of differing viscosities in stirred vessels, *Trans. IChemE.*, 75, 777-783.
- BOUWMANS I. and VAN DEN AKKER, H. E. A., (1990). Influence of viscosity and density differences on mixing times in stirred vessels. *Institute of Chemical Engineers Symposium Series*, 121, 1-12.
- CLEARY, P. W., LAURENT, B. and BRIDGEWATER, J., (2002). DEM prediction of flow patterns and mixing rates in ploughshare mixer. *Proc. of the 4<sup>th</sup> World Cong. on Particle Tech.*, Paper 715.
- CLEARY, P. W. and PRAKASH, M. (2004). Discrete Element Modelling and Smooth Particle Hydrodynamics: potential in the environmental sciences. *Phil. Trans. Roy. Soc. Lond. A*, 362, 2003-2030
- CLEARY, P., HA, J., PRAKASH, M. and NGUYEN, T. (2006). 3D SPH flow predictions and validation for high pressure die casting of automotive components. *App. Math. Model.*, 30, 1406-1427
- COLAGROSSI, A and LANDRINI, M., (2003). Numerical simulations of interfacial flows using smoothed particle hydrodynamics. *J. Comput. Phys.*, 191, 448-475.
- MONAGHAN, J. J., (1992). Smoothed particle hydrodynamics. *Ann. Rev. Astron. Astrophys.*, 30, 543-574.
- MONAGHAN, J. J. and KOCHARYAN, A., (1995). SPH simulation of multi-phase flow. *Comput. Phys. Commun.*, 87, 225–235.
- MONAGHAN, J. J., CAS, R. A. F., KOS, A. M. and HALLWORTH, M., (1999). Gravity currents descending a ramp in a stratified tank. *J. Fluid Mech.*, 379, 39-69.
- PRAKASH, M. and CLEARY, P. W., (2009). Predicting multi-fluid-air-mixing: SPH model development and analysis of mixing dynamics. *Chem. Eng. Sci.*, in preparation.
- ROBINSON, M., CLEARY, P. W. and MONAGHAN, J. J., (2006). Analysis of mixing in a twin-cam mixer using Smoothed Particle Hydrodynamics. *AIChE Journal* 54, no. 8 (2008): 1987-98.
- SMITH, J.M (1990). Industrial needs for mixing research. *Chem. Eng. Res. and Design*, 68, 3-6.
- YEOH, S. L., PAPADAKIS, G. and YIANNESKIS, M. (2005). Determination of mixing time and degree of homogeneity in stirred vessels with large eddy simulation. *Chem. Eng. Sci.*, 60, 2293-2302.
- ZHANG, Z. and CHEN, G., (2007). Chaotic liquid shaker: Design, implementation and application. *Int. J. of Bifurcation and Chaos*, 17, 4443-4451.
- ZHAN, Q., YONG Y., MAO, Z-S., YANG C. and ZHAO C., (2009). Experimental determination and numerical simulation of mixing time in a gas-liquid stirred tank. *Chem. Eng. Sci.*, 64, 2926-2933.